Macromolecules

pubs.acs.org/Macromolecules Article

Crazing Reveals an Entanglement Network in Glassy Ring Polymers

Jiuling Wang and Ting Ge*

Cite This: *Macromolecules* 2021, 54, 7500−7511 Read Online

ACCESS | Metrics & More | Article Recommendations | Supporting Information

ABSTRACT: Molecular simulations are used to show that an entanglement network exists in nonconcatenated ring polymers of sufficiently long contour length when they are cooled down well below the glass transition temperature. The entanglement network consists of only a fraction of the topological constraints that force ring polymers to be in self-similar globular conformations. The entanglement network can support stable craze formation in ring polymer glass under tensile loading. The structural features of the ring polymer craze and the drawing stress during the craze formation are related to the underlying entanglement network by generalizing traditional models for the crazing in linear polymer glass. The computer simulations and theoretical analysis demonstrate tuning polymer topology as a promising way to manipulate the mechanical properties of traditional plastic materials.

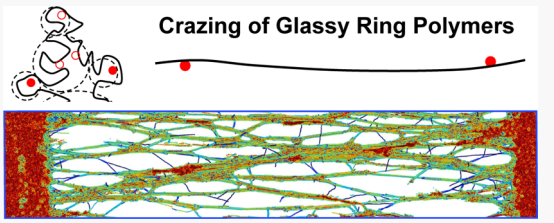

1. INTRODUCTION

Ring polymers with a unique topology exhibit distinctive linear and nonlinear viscoelastic behaviors in the melt and solution states.[1−12] One prominent example is the power-law stress relaxation of nonconcatenated ring polymers[1,2] in contrast to the existence of rubbery plateau in the stress relaxation of entangled linear polymers. The viscoelastic behaviors are intimately related to the static conformations of ring polymers. Recent studies show that nonconcatenated ring polymers have globular conformations due to the topological constraints arising from the noncrossability of different rings.[6,13−21] Meanwhile, ring polymers are not completely segregated from one another but are interpenetrated and threaded by neighboring rings.[2,7,22−28] A recent scaling model[6] of ring polymer conformations and dynamics shows that topological constraints force ring polymers into self-similar loopy globular conformations, but they can be progressively released in such a way that no entanglement network forms to give rise to a rubbery plateau.

The studies of polymer melts and solutions are relevant to the processing of polymer liquids at high temperatures. Nevertheless, the usage of polymeric materials is often at low temperatures, where polymers are in a solid phase.[29−31] A common state of solid polymers is amorphous polymer glass. Conventional wisdom is that polymer glass inherits the entanglement network from the melt state of linear polymers above the glass transition temperature T_g and possesses a mechanical strength governed by the entanglement network. In particular, the entanglement network of linear polymers results in a unique mechanical failure mechanism called crazing in glassy polymers.[32−54] Ahead of the crack tip in a polymer glass, crazes consisting of fibrils and voids grow and greatly increase the fracture toughness by orders of magnitude compared to the prediction based solely on the surface energy required for creating the crack surfaces.[30,33,34,41]

Given the stark contrast between the viscoelastic properties of linear and ring polymer liquids, an intriguing research topic is the consequence of ring topology on the mechanical properties of polymer glasses. Such a study can not only enrich the understanding of topological constraints among ring polymers but also benefit the potential development of ring polymers into useful solid materials.

In this work, we perform molecular dynamics (MD) simulations to initiate the study of large deformation and mechanical failure of ring polymer glasses. Computer simulations have played a significant role in the research on ring polymers as they are able to provide an independent check of experimental observations with perfectly controlled polymer topology as well as detailed analyses of ring polymers at the microscopic level.[2,7,13−17,22−26,55−60] We use the simulations to show that the polymer glass formed by ring polymers of sufficiently long contour length fails through a mechanism similar to the crazing of linear polymer glass. Unlike in the liquid state, the topological constraints on ring polymers can only be partially released in the glassy state upon a large tensile deformation. The unreleased topological constraints lead to an entanglement network that governs the crazing of ring polymer glass. Section 2 describes the simulation model and methods for the preparation and deformation of glassy polymers. Section 3 reports the simulation results and the theoretical

Received: May 18, 2021
Revised: July 13, 2021
Published: August 12, 2021

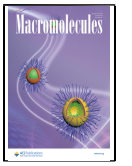

https://doi.org/10.1021/acs.macromol.1c01080
Macromolecules 2021, 54, 7500−7511

analysis by combining the scaling model[6] of ring polymer conformations and the models[32,34−36] of crazing in linear polymer glass. Summary of our findings and concluding remarks are given in Section 4.

2. MODEL AND METHODOLOGY

2.1. Sample Preparation. The simulations employed the conventional bead-spring model[61,62] that captures many features of homopolymers. The van der Waals interactions between monomers of mass m and size σ are modeled using the truncated and shifted Lennard-Jones (LJ) potential

$$U_{\mathrm{LJ}}(r) = \begin{cases} 4\varepsilon\left[\left(\frac{\sigma}{r}\right)^{12} - \left(\frac{\sigma}{r}\right)^{6} - \left(\frac{\sigma}{r_c}\right)^{12} + \left(\frac{\sigma}{r_c}\right)^{6}\right], \\ \quad r \le r_c \\ 0, \qquad r > r_c \end{cases} \tag{1}$$

with the cutoff distance $r_c = 2^{1/6}\sigma$, interaction strength ϵ, and characteristic time $\tau = \sigma\sqrt{m/\varepsilon}$. The bonds between neighboring monomers along the strong covalent backbone of a polymer are modeled by the finite extensible nonlinear elastic (FENE) potential

$$U_{\mathrm{FENE}}(r) = \begin{cases} -\frac{k}{2}{R_0}^2 \ln\left[1 - \left(\frac{r}{R_0}\right)^2\right], & r < R_0 \\ \infty, & r \ge R_0 \end{cases} \tag{2}$$

where the force constant $k = 30\epsilon/\sigma^2$ and the maximum bond length $R_0 = 1.5\sigma$. In addition, adjacent bonds are coupled by a bond bending potential

$$U_{\mathrm{bend}}(\theta) = k_\theta(1 - \cos\theta) \tag{3}$$

where $k_\theta = 1.5\epsilon$ and θ is the angle between the two bonds.

Standard protocols were used to prepare the samples of linear and ring polymers in the melt states with $T = 1.0\epsilon/k_B$, where k_B is the Boltzmann constant. The entanglement length $N_e = 28$ for the linear polymers in the simulations.[63] Chain lengths of the linear polymers are $N_L = 200$ and 800, both of which are much larger than N_e. The rubbery plateaus in the stress relaxations of these well-entangled linear polymers were shown in previous simulations.[2] Contour lengths of the ring polymers are $N_R = 200$, 400, 800, and 1600. Both the self-similar conformations and power-law stress relaxation of these ring polymers were studied by previous simulations.[2,15] Table 1

Table 1. Parameters for Simulation Samples

ring polymer	chain length N_R	200	400	800	1600
	number of chains n_{ch}	1600	1600	1600	800
linear polymer	chain length N_L	200	800		
	number of chains n_{ch}	6400	1600		

lists the number of chains n_{ch} for each N_L or N_R. Periodic boundary conditions were applied to the x-, y-, and z-directions of a sample. The velocity Verlet algorithm was utilized to perform time integration with a time step $\delta t = 0.005\tau$. For linear polymer melts, the double-bridging algorithm[64] was used to equilibrate the polymers. For ring polymer melts, the initial samples with $n_{ch} = 200$ were obtained from Halverson *et al.*[2,15] The samples were enlarged by replicating the ring polymers in a larger simulation box and then equilibrated at $T = 1.0\epsilon/k_B$ for a time period longer than the diffusion time of the rings.[2]

The equilibrated polymer melts were then cooled down to obtain glassy polymers. Prior to the cooling, the FENE bonding potential was replaced with the breakable quartic potential[41,42,65−71]

$$U_{\mathrm{quartic}}(r) = k_1(r - R_1)^3(r - R_2) \tag{4}$$

where $k_1 = 2351\epsilon/\sigma^4$, $R_1 = 1.5\sigma$, and $R_2 = 0.7575\sigma$. These parameters ensure that the equilibrium bond length $l_0 = 0.96\sigma$ is the same as that of the FENE bonds, and the maximum force before a bond breaks is 100 times higher than that required to separate two atoms interacting *via* the LJ potential, which is in the typical experimental range.[72,73] The use of the breakable bonds enables chain scission in the simulations of mechanical failure. Additionally, the attractive part of the LJ potential was turned on by setting the cutoff distance at $r_c = 1.5\sigma$. The same r_c was used in previous simulations that have reproduced many experimental features of the crazing in linear polymer glass.[41,42,52,68,74,75] Despite the changes in the interaction details of the simulation model, the topological constraints among polymers were not altered. A fast quenching preserved the topological constraints. The polymer melt samples were first quenched at a cooling rate of $-9 \times 10^{-4}\epsilon/(k_B\tau)$ and a constant volume from $T = 1.0\epsilon/k_B$ to $T = 0.55\epsilon/k_B$, where the pressure $P = 0$. Subsequently, the samples were quenched at a cooling rate of $-2 \times 10^{-4}\epsilon/(k_B\tau)$ and a constant pressure $P = 0$ from $T = 0.55\epsilon/k_B$ to $T = 0.2\epsilon/k_B$. The Nosé−Hoover thermostat and Nosé−Hoover barostat were used to control the temperature and pressure with the damping parameters 1τ and 50τ, respectively. The glass transition temperature T_g of all samples is $\approx 0.39\epsilon/k_B$, as determined from the specific volume versus temperature plots shown in Figure S1 of Supporting Information. Note that the change of polymer topology from the linear to ring forms does not alter T_g.

2.2. Crazing Simulation. The glass samples at $T = 0.2\epsilon/k_B$ well below T_g were used in crazing simulations. The deformation protocol in the crazing simulations was the same as in previous simulations.[41,42,52,68,70,71] The box dimensions L_x and L_y along the x- and y-directions were kept constant, while the box dimension L_z along the z-direction was increased. This leads to initial triaxial tensile stresses, which are generally required to induce cavitation and subsequent crazing of polymer glasses.[32,76] The deformation rate was increased gradually. At the beginning of the simulation, the deformation rate (engineering strain rate) was set at $(\mathrm{d}L_z/\mathrm{d}t)/L_z^0 = 10^{-5}\tau^{-1}$ until the engineering strain reached $\Delta L_z/L_z^0 = 0.025$, where L_z^0 is the initial box size along the z-direction. Then, the deformation rate was increased to $(\mathrm{d}L_z/\mathrm{d}t)/L_z^0 = 5 \times 10^{-5}\tau^{-1}$ until $\Delta L_z/L_z^0 = 0.1$. Finally, the deformation rate was held constant at $(\mathrm{d}L_z/\mathrm{d}t)/L_z^0 = 2.5 \times 10^{-4}\tau^{-1}$. The deformation rates are in the range where the stress level exhibits a weak logarithmic dependence on the deformation rate.[42] We recorded the tensile stress σ_z as a function of the stretch factor $\lambda = L_z/L_z^0$. A Langevin thermostat with $T = 0.2\epsilon/k_B$ and the damping parameter 1τ was applied to x- and y-directions perpendicular to the stretching direction during the deformation process. All the simulations were performed using the LAMMPS package.[77] Snapshots of glassy polymers during the deformation are shown in Figure 1. For both linear polymers with $N_L = 800$ and ring polymers with $N_R = 800$, a region of crazes formed between two dense glassy

https://doi.org/10.1021/acs.macromol.1c01080
Macromolecules 2021, 54, 7500−7511

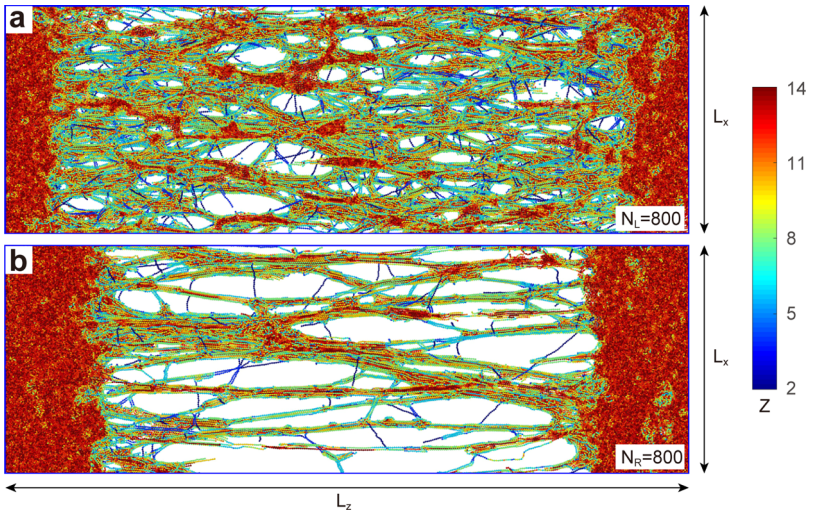

Figure 1. Snapshots of the coexistence of crazed and uncrazed regions for (a) linear (N_L = 800) and (b) ring (N_R = 800) polymers at $T = 0.2\epsilon/k_B$. In both cases, $L_x = 109\sigma$, $L_z = \lambda L_z^0$ with $L_z^0 = 109\sigma$, and the stretch factor $\lambda = 3$. The polymer beads are colored based on the coordination number Z. For clarity, only beads in a slab of thickness 30σ in the y direction are shown.

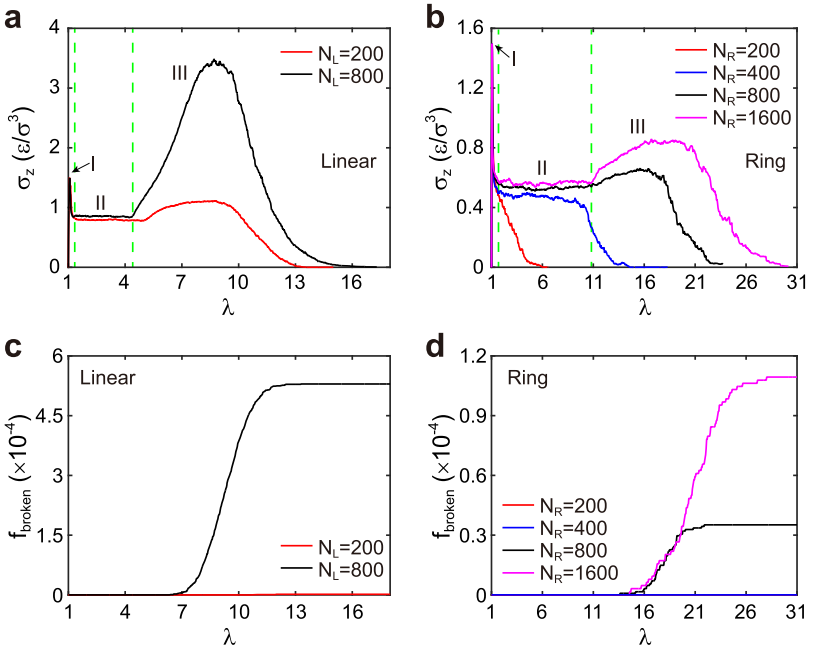

Figure 2. Stress σ_z in the stretching direction as a function of the stretch factor λ for (a) linear and (b) ring polymers. Regimes I (nucleation), II (growth), and III (breakdown) of the crazing process are separated by dashed green lines. The corresponding changes in the fraction f_{broken} of broken bonds are shown in (c,d) for the linear and ring polymers, respectively.

regions. The polymer beads in Figure 1 are colored based on the coordination number Z, which is the number of neighboring beads of a bead. The probability distributions $P(Z)$ for the undeformed glass and the fully developed craze are shown in Figure S2 of Supporting Information.

3. RESULTS AND DISCUSSION

3.1. Stress−Strain Behavior. The plot of tensile stress σ_z as a function of λ for the crazing in linear polymer glass exhibits features in agreement with previous simulations. As shown in Figure 2a, σ_z rises to the yield peak and then drops as the craze nucleates in regime I, it remains at a constant value S as the glass is progressively transformed to craze fibrils in regime II, and eventually, it rises to a second peak, followed by a drop as the entire craze is further stretched and broken in regime III. A stable craze grows in the two linear polymer glasses with N_L = 200 and 800 as the chains are sufficiently long to avoid the catastrophic pullout through chain ends. Nevertheless, the failure mechanism of the developed craze differs in the two samples. The craze for N_L = 200 fails through chain pullout with almost no bond breaking, while the one for N_L = 800 fails through chain scission, as demonstrated by the change in the fraction of broken bonds f_{broken} with increasing λ in Figure 2c. The simulation results in Figure 2a for linear polymer glass agree with the previous results[42,74,78−81] that $N_L \approx 3N_e$ is the threshold for a stable craze formation with a plateau stress S, whereas $N_L \approx 10N_e$ is the threshold for the failure dominated by chain scission.

https://doi.org/10.1021/acs.macromol.1c01080
Macromolecules 2021, 54, 7500−7511

The stress−stretch curves for ring polymer glasses in Figure 2b exhibit features similar to the results in Figure 2a. For all N_R, the peak stress $1.5\epsilon/\sigma^3$ in regime I is the same as that for linear polymers, showing that craze nucleation is not affected by the change in polymer topology. For $N_R = 200$, σ_z quickly drops after regime I, indicating pullout of rings upon deformation and thus no stable craze growth. For $N_R = 400$, a stress plateau emerges after regime I, but it is not fully developed as the ring contour length is still not long enough. For both $N_R = 800$ and $N_R = 1600$, three regimes exist as in the crazing of linear polymer glass (Figure 2a). The stress plateau in regime II is well developed, and the ultimate failure in regime III involves chain scission, as indicated by the increase of f_{broken} with λ in Figure 2d. To conclude, the simulations demonstrate glassy ring polymers of sufficiently long contour length can fail through crazing.

3.2. Extension Ratio. A polymer craze is characterized by the extension ratio $\Lambda = \rho_{uncraze}/\rho_{craze}$, where $\rho_{uncraze}$ and ρ_{craze} are the densities in the uncrazed and crazed regions, respectively. The density profiles at different λ for the linear polymers with $N_L = 800$ and ring polymers with $N_R = 800$ and $N_R = 1600$ are shown in Figure S3 of Supporting Information. We determine that the extension ratio $\Lambda_L = 4.4$ for $N_L = 800$, while $\Lambda_R = 11.5$ and 11.3 for $N_R = 800$ and 1600, respectively. Λ and other properties for linear and ring polymer crazes are listed in Table 2. Λ coincides with the end of regime II, where all dense glass has just been converted to craze fibrils. From the end of regime II in Figure 2, $\Lambda_L = 4.4$ for $N_L = 800$, while $\Lambda_R = 11.0$ for $N_R = 800$ and 1600.

Table 2. Comparison of the Properties for Linear and Ring Polymer Crazes

	extension ratio Λ	scaling relation for Λ	N_e or N_e^R	fibril diameter $\langle D\rangle$ (σ)	fibril diameter $\langle D_{grid}\rangle$ (σ)
$N_L = 800$	4.4	$N_e^{1/2}$	28	5.4	2.7
$N_R = 800$	11.5	$(N_e^R)^{2/3}/N_e^{1/6}$	120	5.3	3.1
$N_R = 1600$	11.3	$(N_e^R)^{2/3}/N_e^{1/6}$	120	5.3	3.1
	fibril spacing $\langle D_0\rangle$ (σ)	drawing stress S (ϵ/σ^3)	$\lambda_{failure}$	work of failure (ϵ/σ^3)	
$N_L = 800$	13.4	0.85	8.7	20.9	
$N_R = 800$	20.2	0.53	16.5	10.9	
$N_R = 1600$	20.4	0.56	19	15.8	

For linear polymer glass, Λ_L has been related to the underlying entanglement network. Kramer first developed the geometric argument[32,34] that Λ_L is determined by the maximum extension of a network strand between entanglements. The argument is rephrased below. Consider a network strand consisting of N_e monomers of size b, the maximum extension $\lambda_{max}^L = l_e^L/d_e^L = N_e b/N_e^{1/2} b = N_e^{1/2}$, where $l_e^L = N_e b$ is the contour length of a strand and $d_e^L = N_e^{1/2} b$ is the root-mean-squared (rms) end-to-end size of a strand according to the Gaussian chain statistics. For simplicity, the characteristic ratio C_∞ is dropped from the expression of d_e^L. The proportionality between Λ_L and λ_{max}^L for linear polymers has been confirmed by experiments and simulations.[32,34,42,52,75]

For glassy ring polymers of sufficiently long contour length, the stable growth of the craze indicates the existence of an underlying entanglement network. We develop a geometric argument similar to Kramer's to relate Λ_R to the entanglement network in glassy ring polymers. As illustrated in Figure 3a, the topological constraints indicated by the open and filled red circles force a ring polymer to be in a self-similar loopy globular conformation, but only the topological constraints indicated by the filled red circles contribute to the entanglement network in glassy ring polymers. A network strand is indicated by the black line between the two filled red circles within the blue dashed rectangular box in Figure 3a. The network strand is a compact three-dimensional object made of N_e^R/N_e "elementary loops", where N_e is the average number of monomers in an elementary loop between two topological constraints, and $N_e^R > N_e$ is the average number of monomers in a network strand. For simplicity, the entanglement length N_e for linear polymers is used as the average number of monomers between topological constraints. The rms end-to-end size of an elementary loop is $N_e^{1/2} b$, corresponding to a Gaussian chain conformation between two topological constraints. Here, again the characteristic ratio C_∞ is dropped from the expression for the elementary loop size. A recent study[21] has demonstrated that the size of an elementary loop of ring polymers is in the range of an entanglement strand size N_e for linear polymer melts and characterized by Gaussian statistics. The rms end-to-end size of a network strand is $d_e^R = (N_e^R/N_e)^{1/3} \cdot (N_e^{1/2} b)$, corresponding to the self-similar conformation of rings. As illustrated in Figure 3b, the maximum extension of the strand with contour length $l_e^R = N_e^R b$ is $\lambda_{max}^R = l_e^R/d_e^R = (N_e^R)^{2/3}/N_e^{1/6}$.

Based on $\Lambda_L = \lambda_{max}^L = N_e^{1/2}$ from Kramer's geometric argument for linear polymer glass and $\Lambda_R = \lambda_{max}^R = (N_e^R)^{2/3}/N_e^{1/6}$ from our geometric argument for ring polymer glass, we obtain $N_e^R = N_e(\Lambda_R/\Lambda_L)^{3/2}$, a relation that allows us to estimate N_e^R from the known value of N_e and the measured values of Λ_R and Λ_L. Note that C_∞ does not enter $\lambda_{max}^R/\lambda_{max}^L$ and the relation $N_e^R = N_e(\Lambda_R/\Lambda_L)^{3/2}$. Using $N_e = 28$, $\Lambda_R = 11.5$, and $\Lambda_L = 4.4$, we estimate that $N_e^R = 120 \approx 4.3 N_e$. This result indicates that on average, only one out of four topological constraints that determine the conformations of ring polymers contribute to the formation of an entanglement network that supports the craze growth in the glassy state. Using the estimated value of N_e^R, we further examine the results in Figure 2b. No stable craze forms for $N_R = 200 < 3N_e^R$, a stable craze starts to emerge for $N_R = 400 \approx 3N_e^R$, while stable crazes form for $N_R = 800 > 3N_e^R$ and $N_R = 1600 > 3N_e^R$. The threshold for stable craze growth in ring polymer glass is $N_R \approx 3N_e^R$, in agreement with the threshold $N_L \approx 3N_e$ established for linear polymer glass. For both linear and ring polymers, the physical meaning of the threshold is that a few entanglements per polymer are needed to prevent the catastrophic pullout of polymers and thus promote stable craze growth.

Figure 3c,d visualizes the conformational changes of ring polymers during craze formation in the simulations. An ensemble of 200 ring polymers of $N_R = 800$ is visualized with their centers of mass overlapping with each other. One ring polymer with its squared radius of gyration R_g^2 closest to the average $\langle R_g^2\rangle$ for the 200 ring polymers in the undeformed glassy state is highlighted. The polymer beads in the highlighted ring are colored based on their positions in the ring. The conformational changes of the color-coded ring polymer during craze formation align with the schematic illustration in Figure 3a,b. A quantitative comparison of the conformational changes of a network strand in the schematic illustration and those in the simulations are not feasible without identifying and tracking individual topological

https://doi.org/10.1021/acs.macromol.1c01080
Macromolecules 2021, 54, 7500−7511

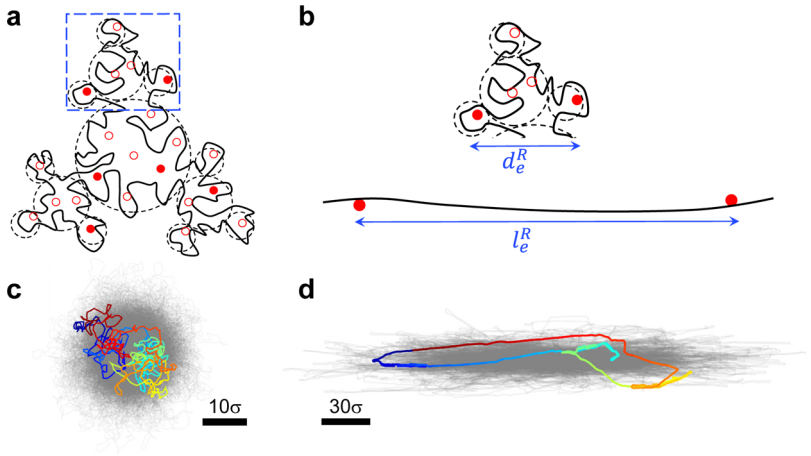

Figure 3. (a) Schematic illustration of the self-similar conformation of a ring polymer (solid black line) under topological constraints (open and filled red circles). Loops at different length scales are indicated by dashed black circles. A fraction of the topological constraints (filled red circles) form an entanglement network in glassy ring polymers. The blue dashed rectangular box encloses one network strand. (b) The maximum extension of an entanglement network strand is $\Lambda_R = l_e^R/d_e^R$, where l_e^R is the contour length of a strand and d_e^R is the rms end-to-end size of a strand. (c,d) Snapshots of an ensemble of 200 ring polymers of $N_R = 800$ in (c) undeformed glassy state at $\lambda = 1$ and (d) fully developed craze at $\lambda = 12$. The centers of mass of the 200 ring polymers are shifted to overlap. One ring polymer is highlighted by coloring the polymer beads based on their positions in the ring. In the undeformed glassy state, the squared radius of gyration R_g^2 of the highlighted ring is the closest to the average $\langle R_g^2 \rangle$ of the 200 rings. The same ring polymer is highlighted in (c,d). Note the change of the scale bar from (c) to (d).

constraints in the simulations. Sophisticated algorithms of geometric analysis such as the contour reduction analysis (CReTA) algorithm[82,83] may be applied to the trajectories of ring polymer crazing in the future.

3.3. Craze Structure. A polymer craze consists of fibrils and voids, as illustrated in Figure 1. To quantify the craze structure, we compute the fibril diameter and the spacing between fibrils. A fully developed craze at the end of regime II was divided into consecutive slices of thickness $\delta L_z = r_c = 1.5\sigma$ along the z-direction. The monomers in one slice were projected to the xy-plane and grouped into clusters to represent the cross sections of craze fibrils. Two monomers are in the same cluster if their separation is smaller than $r_c = 1.5\sigma$. Figure 4a,b shows the cross sections of the linear polymer craze and ring polymer craze, respectively. The diameter of a fibril is related to the area A of a cluster as $D = \sqrt{4A/\pi}$. To obtain the area A for each cluster, the xy-plane was divided into a grid of square cells with the side length of a cell $a_0 = 0.2\sigma$. The area A of a cluster is the sum of the area of all square cells that are within $\delta r = r_c/2 = 0.75\sigma$ from at least one bead in the cluster. The average spacing between fibrils is estimated as $\langle D_0 \rangle = \sqrt{4L_xL_y/(\pi\langle m \rangle)}$, where $\langle m \rangle$ is the average number of clusters per slice.

The calculation of the fibril diameter as $D = \sqrt{4A/\pi}$ is based on the approximation of a fibril cross section as a circle, which corresponds to the ideal treatment of craze fibrils as uniform vertical cylinders in the molecular models of crazing. To go beyond the approximation, we calculate the fibril diameter using a different method that takes into account the anisotropic shape of a fibril cross section. As illustrated in Figure 4c, we find all the horizontal and vertical straight lines across the fibril cross section on the grid of square cells and determine the length l_{grid} of each line. The average of l_{grid} is the effective diameter D_{grid} of the fibril. By sampling l_{grid} from different positions and orientations, this approach captures the effect of the anisotropic shape on the fibril diameter. The fibril area A, fibril diameter D_{grid}, and fibril perimeter P are related to each other as $A = P \cdot D_{grid}/\pi$.[84] The grid cells that belong to a fibril cross section but have less than four nearest neighbors in the same cross section constitute the perimeter of the cross section. The perimeter $P = \beta a_0 N_p$, where N_p is the number of the cells on the perimeter and $\beta = 1.1222$ is a numerical correction factor.[84] Figure 4d shows that the relation $A = P \cdot D_{grid}/\pi$ holds in our system, justifying the estimation of the fibril diameter.

The probability distributions $P(D)$ and $P(D_{grid})$ for the fully developed crazes are shown in Figure 4e,f, respectively. The number-average fibril diameter $\langle D \rangle^R = 5.3\sigma$ for the ring polymers is close to $\langle D \rangle^L = 5.4\sigma$ for the linear polymers. However, the area-average fibril diameter $\langle D \rangle_A^R = 8.9\sigma$ for the ring polymers is smaller than $\langle D \rangle_A^L = 11.8\sigma$ for the linear polymers, in consistency with the less dispersed distribution of D in Figure 4e. The number-average fibril diameter $\langle D_{grid} \rangle^R = 3.1\sigma$ for the ring polymer craze is also close to $\langle D_{grid} \rangle^L = 2.7\sigma$ for the linear polymer craze, consistent with the result based on the approximation of a cross section as a circle. Interestingly, the area-average fibril diameter $\langle D_{grid} \rangle_A^R = 4.4\sigma$ is larger than $\langle D_{grid} \rangle_A^L = 4.2\sigma$, which is different from the result $\langle D \rangle_A^R < \langle D \rangle_A^L$, reflecting the effect of the anisotropic shape of the cross section.

The average spacing between fibrils $\langle D_0 \rangle^R = 20.2\sigma$ for the ring polymers is larger than $\langle D_0 \rangle^L = 13.4\sigma$ for the linear polymers. The larger separation between craze fibrils in ring polymers compared to that in linear polymers is also observed in Figure 1. For the craze in linear polymer glass, it has been argued that $\langle D_0 \rangle^L$ is determined by the average spacing between entanglements or the rms end-to-end size of a strand in the entanglement network as the growth of a void during crazing is limited by the network strands.[35,36] According to this argument, $\langle D_0 \rangle^L = d_e^L = N_e^{1/2} b$ for linear polymers. The same argument applied to ring polymer glass gives $\langle D_0 \rangle^R = d_e^R = (N_e^R/N_e)^{1/3} \cdot (N_e^{1/2} b)$. With $N_e^R = 120$ and $N_e = 28$, the geometric argument leads to $\langle D_0 \rangle^R / \langle D_0 \rangle^L = (N_e^R/N_e)^{1/3} = 1.62$. This ratio from relating $\langle D_0 \rangle$ to the rms end-to-end size of an entanglement network strand is close to $\langle D_0 \rangle^R / \langle D_0 \rangle^L =$

https://doi.org/10.1021/acs.macromol.1c01080
Macromolecules 2021, 54, 7500−7511

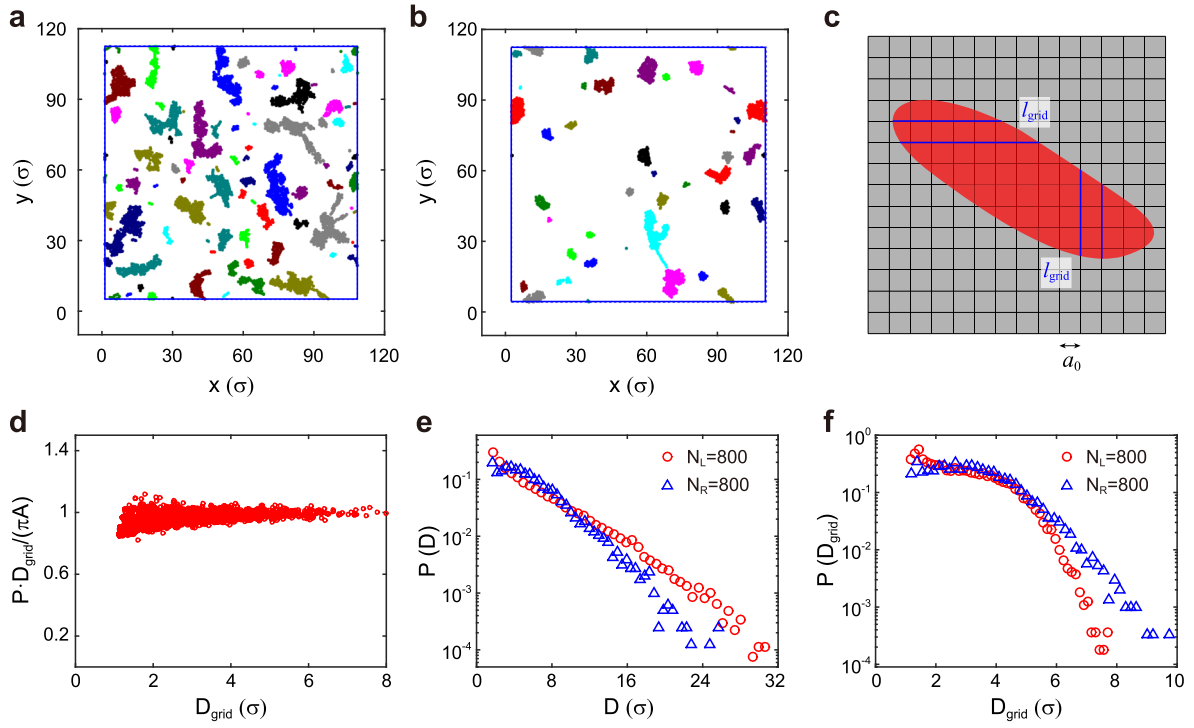

Figure 4. Cross section of a fully-developed craze in (a) linear polymers of $N_L = 800$ at $\lambda = 5$ and (b) ring polymers of $N_R = 800$ at $\lambda = 12$. The blue squares in (a,b) indicate the simulation boxes with periodic boundary conditions. (c) Schematic illustration of a fibril cross section (red cluster) and four lines (blue lines) across it. l_{grid} denotes the length of a line, and the average of l_{grid} for all lines across the cluster is the fibril diameter D_{grid}. (d) $P{\cdot}D_{grid}/(\pi A)$ as a function of D_{grid} for the ring polymer craze with $N_R = 800$. (e,f) Probability density functions $P(D)$ and $P(D_{grid})$ for the linear ($N_L = 800$) and ring ($N_R = 800$) polymer crazes.

$20.2\sigma/13.4\sigma = 1.51$ from the analysis of the craze structure, supporting the argument that $\langle D_0\rangle$ is determined by the average spacing between entanglements. For linear polymers, the entanglement length N_e can be tuned by diluting the polymers with short unentangled chains, and it was found that an increased N_e leads to a larger fibril spacing $\langle D_0\rangle$,[85] which is consistent with our results here.

$\langle D\rangle$ can also be related to the entanglement network. Consider one slice of the fully developed craze; the area occupied by craze fibrils is L_xL_y/Λ, which is reduced by Λ with respect to L_xL_y for the same slice across the uncrazed glass. The average number of fibrils $\langle m\rangle = L_xL_y/(\pi\langle D_0\rangle^2/4)$, the area per fibril $A = (L_xL_y/\Lambda)/\langle m\rangle = \pi\langle D_0\rangle^2/4\Lambda$, and therefore, the average fibril diameter $\langle D\rangle = \sqrt{4A/\pi} = \langle D_0\rangle/\sqrt{\Lambda}$. Using $\langle D_0\rangle^R/\langle D_0\rangle^L = (N_e^R/N_e)^{1/3}$ and $\Lambda_R/\Lambda_L = (N_e^R/N_e)^{2/3}$, we obtain $\langle D\rangle^R/\langle D\rangle^L = (\langle D_0\rangle^R/\langle D_0\rangle^L)/\sqrt{\Lambda_R/\Lambda_L} = 1$, meaning the same average fibril diameter for linear and ring polymer crazes. This result based on the geometric argument above agrees with $\langle D\rangle^R = 5.3\sigma$ and $\langle D\rangle^L = 5.4\sigma$ from the analysis of the craze structure. The geometric argument may be extended to explain the result that $\langle D_{grid}\rangle^R = 3.1\sigma$ and $\langle D_{grid}\rangle^L = 2.7\sigma$ are almost the same by introducing a prefactor α correcting for the anisotropic shape of a fibril cross section. According to our calculation, $\langle D_{grid}\rangle = \alpha\langle D\rangle$ with $\alpha = 0.5-0.6$.

3.4. Drawing Stress. The growth of the craze in regime II occurs under a constant drawing stress S for both linear and ring polymers. $S_R = 0.53\epsilon/\sigma^3$ for the ring polymers of $N_R = 800$ is below $S_L = 0.85\epsilon/\sigma^3$ for the linear polymers of $N_L = 800$, as shown in Figure 2. However, the decomposition of local drawing stress $s(z)$ to bonded and nonbonded components exhibits similar features in both linear and ring polymers. As shown in Figure 5a,b, there are interfaces between the uncrazed region and the crazed region, which are the active zones for the conversion of dense glass to craze fibrils. While $s(z) = S$ is independent of z, the dominant component of $s(z)$ changes from the nonbonded stress mainly due to the pairwise LJ interactions in the uncrazed region to the bonded stress carried by the covalent bonds in the crazed region. The changes of the dominant component across the active zone are shown in Figure 5c,d.

The drawing stress acts to pull polymers out of the dense glass and turn them into craze fibrils. Across the active zone, there is a balance of the bonded stress in the crazed region and the nonbonded stress in the uncrazed region, the latter of which is directly related to the creation of new surfaces in the glass. Traditionally, the drawing process has been modeled as the propagation of voids into the region of dense glass, as in the pioneering studies by Kramer and Berger[32,34] and the subsequent work by Krupenkin and Fredrickson.[35,36] The drawing stress S is related to the energy Γ required to create a unit new surface in the glass and the radius of curvature of a void front, which is proportional to the average spacing $\langle D_0\rangle$ between fibrils. With the numerical prefactor dropped, $S \approx \Gamma/\langle D_0\rangle$, one would expect that Γ is not affected by the topology of polymers at the chain level. We estimate the surface energy as $\Gamma = \Delta U_{LJ}/A_s$, where ΔU_{LJ} is the increase in the nonbonded LJ potential energy due to the creation of the craze fibril surface and A_s is the surface area of all craze fibrils at the end of regime II. $A_s = \int_0^{L_z} P_t(z)\,dz$, where $P_t(z)$ is the sum of the perimeters of all fibril cross sections located at z, and the perimeter P of a cross section is computed using the procedure described in Section 3.3. We find that the surface area of the

https://doi.org/10.1021/acs.macromol.1c01080
Macromolecules 2021, 54, 7500−7511

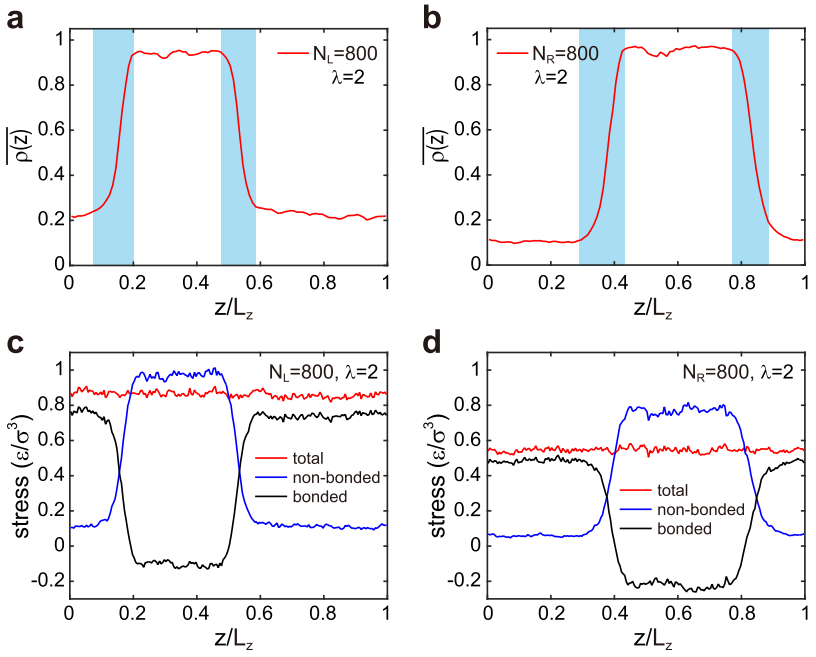

Figure 5. Normalized density $\overline{\rho(z)} = \rho(z)/\rho_{glass}$ *vs* z/L_z for (a) linear polymers and (b) ring polymers at $\lambda = 2$. $\rho_{glass} = 0.993\sigma^{-3}$ is the density of polymer glass before deformation. The blue shaded regions indicate the active zones. Total local drawing stress $s(z)$ and the contributions from bonded and nonbonded interactions *vs* z/L_z for (c) linear and (d) ring polymers. The bonded stress includes the contributions from the bonding and bond bending potentials. The nonbonded stress includes the contribution from the LJ potential. The kinetic contribution to $s(z)$ has been equally split into bonded and nonbonded components. For clarity, the dense uncrazed region has been shifted to the center of the periodic simulation box.

linear polymer craze $A_s^L = 1.31 \times 10^6\sigma^2$ is slightly larger than that of the ring polymer craze $A_s^R = 1.16 \times 10^6\sigma^2$, which is consistent with the result that the average coordination number $\overline{Z_L} = 9.8$ for the linear polymer craze is slightly smaller than $\overline{Z_R} = 10.5$ for the ring polymer craze in Figure S2 of Supporting Information. The estimated surface energies for the linear and ring polymers are $\Gamma^L = 0.77\epsilon/\sigma^2$ and $\Gamma^R = 0.64\epsilon/\sigma^2$, respectively. Γ for the two systems are close to each other, and both agree with the polymer−vacuum interfacial energy $\Gamma = 0.6 - 1.0\epsilon/\sigma^2$ determined by previous simulations.[41,74] Application of the void propagation model to ring and linear polymers in the simulations leads to $S_R/S_L = (\Gamma^R/\Gamma^L)\cdot(\langle D_0\rangle^R/\langle D_0\rangle^L)^{-1} = 0.55$. The result is close to $S_R/S_L = (0.53\epsilon/\sigma^3)/(0.85\epsilon/\sigma^3) = 0.62$ from Figure 2. Therefore, the difference between S_R and S_L can be explained as the consequence of the different average sizes $\langle D_0\rangle$ of voids between the fibrils. Furthermore, as $\langle D_0\rangle^L = N_e^{1/2}b$ for linear polymers and $\langle D_0\rangle^R = (N_e^R/N_e)^{1/3}\cdot(N_e^{1/2}b)$ for ring polymers, $S_R/S_L \sim (N_e^R/N_e)^{-1/3}$ for $\Gamma^R = \Gamma^L$, indicating that the plateau stress ratio is related to the entanglement networks.

We further examine the thermodynamics in the conversion of dense glass to craze fibrils. The total work done in regime II is $W \approx S(L_xL_y)(\Lambda - 1)$. The potential energy change ΔU during craze formation includes the contributions from the changes in the bond, angle, and pairwise LJ interactions. ΔU as a function of λ is shown in Figure S4 of Supporting Information. Since there is no change in the kinetic energy at constant T, the work dissipated as heat is calculated as $Q = W - \Delta U$. We find that $Q/W = 88\%$, 97%, and 96% for $N_L = 800$, $N_R = 800$, and $N_R = 1600$, respectively. The large fraction of the work dissipated as heat is related to the rearrangements of LJ interactions between monomers as the chains are converted to the fibrils with open surfaces.

3.5. Perturbative Simulations. Our interpretation of the simulation results of crazing in ring polymer glass is based on the entanglement network with network strand length N_e^R, which controls Λ_R, $\langle D\rangle^R$, and $\langle D_0\rangle^R$ according to the geometric arguments for the craze structure, and S according to the void propagation model for craze growth. Perturbative computer simulations are designed to further explore the entanglement network. In a set of perturbative simulations, we removed n_{cut} bonds that are regularly distributed along the contour of a ring polymer and thereby cut each ring into n_{cut} linear subsections with length $N_{sub} = N_R/n_{cut}$, as illustrated in Figure 6a. The stress−stretch curves in Figure 6b show that stable craze formation occurs only if $N_{sub} \geq 400$. For $N_{sub} = 200 < 3N_e^R$, there are no sufficient entanglements to prevent the catastrophic pullout from the open chain ends. $N_{sub} = 400 \approx 3N_e^R$ is the marginal case where regime II is almost fully developed. For $N_{sub} = 800 > 3N_e^R$ and $N_{sub} = 1600 > 3N_e^R$, there are sufficient entanglements per chain to yield an entanglement network and support the stable craze growth. The resulting stable craze forms only for $N_{sub} > 3N_e^R$, further demonstrating the role of N_e^R as an effective entanglement length for ring polymer crazing. Figure 6b for different N_{sub} aligns with Figure 2b for different N_R, reflecting that the subsections of large rings behave as smaller rings due to the self-similar conformations of ring polymers. For $N_{sub} \geq 400$, both the extension ratio of the craze and the constant drawing stress during craze formation are almost the same in different samples. This excludes the formation of topological links under tension as the origin of ring polymer crazing. The conjecture that topological links between nonconcatenated rings might emerge is motivated by a recent study[11] that demonstrates that topological links play a critical role in the thickening of ring polymer melts under weak extensional flow. Driven by the flow, topological links form

https://doi.org/10.1021/acs.macromol.1c01080
Macromolecules 2021, 54, 7500−7511

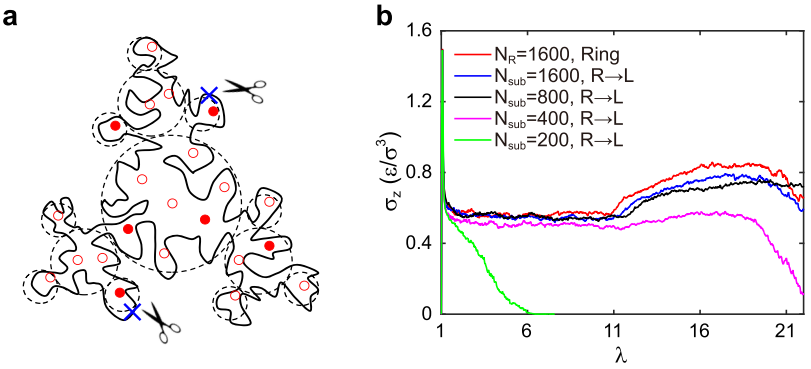

Figure 6. (a) Illustration of cutting of one ring polymer into n_{cut} linear subchains with chain length $N_{sub} = N_R/n_{cut}$. (b) Stress σ_z in the elongation direction for the ring polymers ($N_R = 1600$) and the newly created linear polymers.

between ring polymers and connect multiple rings into supramolecular chains[11] that induce the thickening behavior. Such a phenomenon cannot occur for the linear subsections in Figure 6, where the ring topology is broken by the open ends, and thus cannot play a role in the stable craze formation.

In another set of perturbative simulations, we fixed n_{fix} monomers that are regularly distributed along the contour of a ring polymer and turned each ring into n_{fix} subsections of length $N_{sub} = N_R/n_{fix}$ with fixed ends, as illustrated in Figure 7a. We then introduced internal tension to pull the subsections as taut as possible without allowing them to cross each other. The thick green lines in Figure 7a indicate the taut subsections between fixed monomers after the process. This procedure is similar to the standard algorithm of primitive path analysis.[63] Technically, we turned off all the intrachain LJ and bond-bending potentials and then ran simulations with the fixed monomers at $T = 0.01\epsilon/k_B$ (close to zero) until the system energy was minimized. A Langevin thermostat was used to control T, and the friction constant was $20\tau^{-1}$ during the first 1000 time steps and $0.5\tau^{-1}$ afterward.[62] The perturbative simulations with fixed monomers were also performed for the linear polymers with $N_L = 800$. Two chain ends were always fixed, and the rest $(n_{fix} - 2)$ fixed monomers were regularly distributed along the chain. In particular, the simulation with only two chain ends fixed $(n_{fix} = 2)$ is exactly the primitive path analysis.

Figure 7b shows the rms end-to-end size $\langle R^2(n)\rangle^{1/2}$ of a subsection as a function of the number of monomers n in a subsection for linear polymers of $N_L = 800$ in the melt state and after the perturbative simulations with $n_{fix} = 2$, 3, 5, and 9 fixed monomers per chain. In the melt state, there is a crossover from $\langle R^2(n)\rangle^{1/2} \sim n$ to $\langle R^2(n)\rangle^{1/2} \sim n^{1/2}$, corresponding to the change from a straight segment to a linear chain of random-walk conformation. After a perturbative simulation, $\langle R^2(n)\rangle^{1/2}$ was calculated only for n up to $N_{sub} = N_L/(n_{fix} - 1)$. The results for different n_{fix} almost overlap with each other, exhibiting a crossover from $\langle R^2(n)\rangle^{1/2} \sim n$ to $\langle R^2(n)\rangle^{1/2} \sim n^{1/2}$. As indicated in Figure 7b, the entanglement length $N_e = 28$ is between the two asymptotic regimes. $\langle R^2(n)\rangle^{1/2} \sim n$ for $n < N_e$ describes a straight segment between entanglements, while $\langle R^2(n)\rangle^{1/2} \sim n^{1/2}$ describes the random walk of the straight segment as n exceeds N_e.

Figure 7c shows $\langle R^2(n)\rangle^{1/2}$ for the ring polymers of $N_R = 1600$ in the melt state and after the perturbative simulations with $n_{fix} = 2$, 4, 8, and 16 fixed monomers per ring. Figure 7d shows the snapshots of ring conformations after the perturbative simulations. In the melt state, $\langle R^2(n)\rangle^{1/2} \sim n^{1/3}$ emerges at intermediate n, indicating the self-similar globular conformation of ring polymers. $\langle R^2(n)\rangle^{1/2}$ levels off as n approaches $N_R/2$ due to the finite-size effect. After a perturbative simulation, $\langle R^2(n)\rangle^{1/2}$ was calculated only for n up to $N_{sub} = N_R/n_{fix}$. For $N_{sub} = 100$, $\langle R^2(n)\rangle^{1/2}$ scales almost linearly with n, indicating that almost no entanglements exist at that length scale to resist the pulling by internal tension. For $N_{sub} \geq 200$, there is a sublinear dependence of $\langle R^2(n)\rangle^{1/2}$ on n for sufficiently large n due to the emergence of entanglements. Although a clean asymptotic regime for the sublinear dependence is not observed, the range of n for the sublinear dependence roughly corresponds to n larger than the entanglement length $N_e^R = 120$ of glassy ring polymers. This correspondence essentially reflects the similarity between the topological constraints during the pulling under internal tension and those during the craze formation under tensile loading. Unlike the conformational statistics for the linear polymers after the pulling in Figure 7b, the conformational statistics for the ring polymers after the pulling depends on the value of N_{sub}. This is another difference between topological constraints in the two systems. For ring polymers, the pulling with $n_{fix} = 2$ fixed monomers that are furthest apart from each other in a ring has been performed, and an effective entanglement length N_e^R has been calculated by assuming random-walk statistics for the polymer subsections after the pulling.[2] However, our result in Figure 7c shows that it is not appropriate to estimate N_e^R using the random-walk statistics as the conformational statistics of the subsections of ring polymers after the pulling does not exhibit a clean regime with $\langle R^2(n)\rangle^{1/2} \sim n^{1/2}$ at large n.

3.6. Discussion. The geometric argument for the extension ratio Λ does not take into account the random orientation of the end-to-end vector of an entanglement network strand and the fact that a strand is fully stretched to λ_{max} during craze formation only if the end-to-end vector is aligned with the stretching direction. In fact, the full extension of a polymer backbone, as indicated by the emergence of broken bonds in Figure 2, occurs at a stretch factor λ above the craze extension ratio Λ. As a result, there is a prefactor of order unity that is dropped from the relation $\Lambda = \lambda_{max}$.[32,34,42,52] However, regardless of the exact value of the prefactor, the relation $\Lambda_R/\Lambda_L = \lambda_{max}^R/\lambda_{max}^L$ holds.

The nucleation and growth of craze precede the mechanical failure of glassy polymers. The calculation of the fracture toughness of glassy polymers requires a multiscale approach, as demonstrated previously.[41] Since the focus of this paper is craze formation in regime II, the multiscale approach has not

https://doi.org/10.1021/acs.macromol.1c01080
Macromolecules 2021, 54, 7500−7511

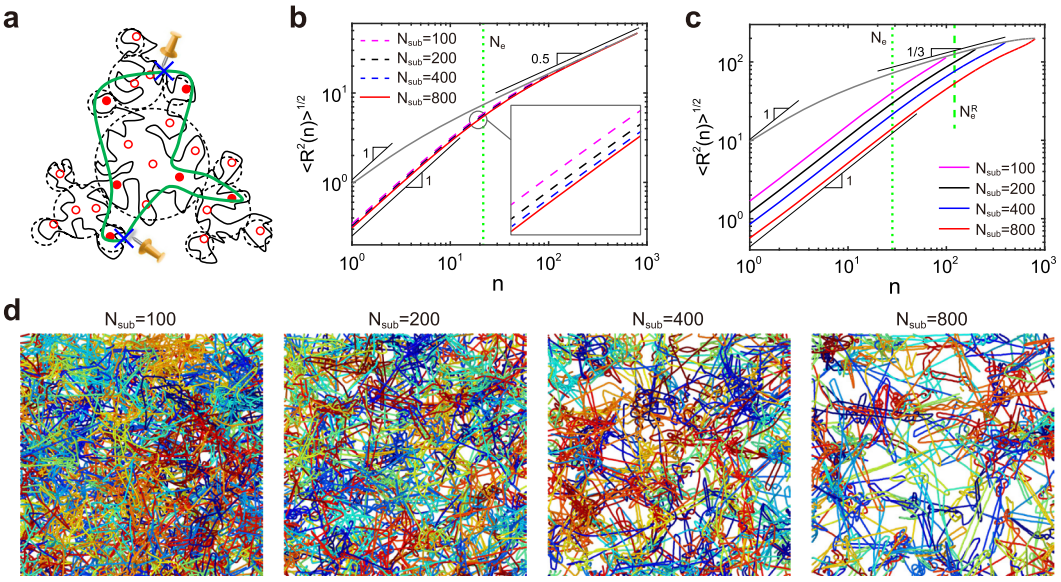

Figure 7. (a) Illustration of fixing n_{fix} monomers in a ring polymer. The thick green lines indicate the taut subsections between fixed monomers after the pulling with internal tension. (b) rms end-to-end size $\langle R^2(n)\rangle^{1/2}$ as a function of the number of monomers n in a subsection for linear polymers of $N_L = 800$. (c) $\langle R^2(n)\rangle^{1/2}$ for ring polymers of $N_R = 1600$. The gray curve shows $\langle R^2(n)\rangle^{1/2}$ in the melt state, while the other curves show $\langle R^2(n)\rangle^{1/2}$ after the perturbative simulations. For linear polymers, $N_{sub} = N_L/(n_{fix} - 1)$, where n_{fix} is the number of fixed monomers per chain. For ring polymers, $N_{sub} = N_R/n_{fix}$. The dotted green lines in (b,c) indicate $N_e = 28$. The dashed green line in (c) indicates $N_e^R = 120$. (d) Snapshots of the ring polymer ($N_R = 1600$) conformations after the perturbative simulations with n_{fix} monomers fixed. For each subfigure, N_{sub} is indicated. For clarity, only polymers within a region of $60\sigma \times 60\sigma \times 60\sigma$ are displayed.

been used to calculate the fracture toughness. However, in Table 2, we report the failure point $\lambda_{failure}$, which corresponds to the peak of the tensile stress in regime III, and the work of failure, which is the integral of the entire stress−stretch curve. The work of failure here is the work done to break the finite-size sample in the simulation and does not represent the fracture toughness of a macroscopic sample.

The glassy state of ring polymers in our simulations arises from the suppression of molecular mobility as the temperature drops below T_g. Glassy states of ring polymers have been created in different ways. For example, by randomly pinning a small fraction of ring polymers, it has been shown that the strong interpenetration between ring polymers can generate an extensive network of topological constraints and thereby induces a kinetically arrested state well above the classical glass transition temperature T_g.[86,87] A recent work has shown that ring polymers can transition into a glassy state also by increasing the mobility of the segments of ring polymers.[88,89] In this work, the traditional approach to prepare a glassy state allows us to borrow the conventional wisdom that topological constraints in glassy polymers are inherited from those in the melt states and thus justify the theoretical description of self-similar globular ring polymer conformations in the glassy state.

For the same contour length, the only difference between linear and ring polymers is their topology and thus topological constraints. Without changing the interactions in the simulation model, the comparison of crazing in linear and ring polymer glasses evaluates the traditional models[32,34−36] of polymer crazing from a new perspective. Previous studies showed that the entanglement network of linear glassy polymers can be tuned by introducing short unentangled chains to dilute the polymers[85,90] or by reducing the thickness of a thin glassy polymer film.[91] This work shows changing polymer topology from linear to ring is an alternative method to alter the entanglement network without changing the chemistry.

On the theoretical side, one open question is what determines the fraction (~1/4 in this work) of the topological constraints that can survive the process of craze formation in the glassy state and serve as the constituents of an entanglement network. Detailed tracking of the evolution of topological constraints during the crazing of ring polymer glass may provide some insights. For the crazing of linear polymer glass, the application of the CReTA algorithm[82,83] to simulation trajectories has revealed that the topological constraints on the linear chains in the glassy state correspond to the rheological tubes restricting chain dynamics in the melt state, rather than acting as permanent cross-links.[52] For the crazing of ring polymers, it would be interesting to check whether a theoretical concept similar to the rheological tube for linear polymers may be introduced to understand the topological constraints that survive the craze formation.

4. CONCLUSIONS

To summarize, we have performed MD simulations to show the crazing of nonconcatenated ring polymers in the glassy state. Our results demonstrate that a fraction of the topological constraints that force ring polymers to be in the self-similar globular conformations can form an entanglement network that supports stable craze formation in ring polymer glass. If the contour length of ring polymers is above 3 times the entanglement strand length N_e^R, a stable craze can form in rings as the catastrophic pullout is inhibited. The maximum extension of an entanglement network strand determines the extension ratio Λ_R of craze fibrils with respect to dense glass. The average network strand size d_e^R determines the average spacing $\langle D_0\rangle^R$ between craze fibrils and thereby the average fibril diameter $\langle D\rangle^R$. Generalizing the geometric argument about the structure of the craze in linear polymer glass to the

https://doi.org/10.1021/acs.macromol.1c01080
Macromolecules 2021, 54, 7500−7511

ring polymer craze allows us to quantitatively describe the relation between the entanglement network and structural features of the ring polymer craze. The constant drawing stress S during craze growth is related to $\langle D_0 \rangle^R$ and therefore d_e^R. The craze growth model based on void propagation allows us to quantitatively account for the change in the drawing stress as the polymer topology changes from linear to ring. The value of N_e^R for the entanglement network in the crazing of ring polymers is further validated by a set of perturbative simulations with open ends introduced and another set of perturbative simulations of pulling internal chain segments with fixed monomers.

We hope that the computational work and theoretical analysis presented here will motivate experimentalists to cool down their ring polymer samples and carry out crazing experiments to confirm our findings. The relation $N_e^R = N_e(\Lambda_R/\Lambda_L)^{3/2}$ can be used to characterize the entanglement network in glassy ring polymers. We anticipate that future computational and theoretical research as well as experiments will further clarify the relation between polymer topology and glassy polymer mechanics, which offers a novel pathway to manipulate the mechanical properties of traditional plastic materials.

■ ASSOCIATED CONTENT

Supporting Information

The Supporting Information is available free of charge at https://pubs.acs.org/doi/10.1021/acs.macromol.1c01080.

Glass transition temperature T_g, coordination number of polymer beads, density profiles during craze growth, and potential energy change during crazing (PDF)

■ AUTHOR INFORMATION

Corresponding Author

Ting Ge − *Department of Chemistry and Biochemistry, University of South Carolina, Columbia, South Carolina 29208, United States;* orcid.org/0000-0003-2456-732X; Email: tingg@mailbox.sc.edu

Author

Jiuling Wang − *Department of Chemistry and Biochemistry, University of South Carolina, Columbia, South Carolina 29208, United States;* orcid.org/0000-0002-7379-3561

Complete contact information is available at: https://pubs.acs.org/10.1021/acs.macromol.1c01080

Notes

The authors declare no competing financial interest.

■ ACKNOWLEDGMENTS

We thank Jonathan Halverson and Gary Grest for sharing the initial ring polymer samples with us. We thank Thomas O'Connor and Gary Grest for helpful discussion. T.G. acknowledges startup funds from the University of South Carolina. This work was supported in part by the National Science Foundation EPSCoR Program under NSF award no. OIA-1655740. Any opinions, findings, and conclusions or recommendations expressed in this material are those of the authors and do not necessarily reflect those of the National Science Foundation. Computational resources were provided by the University of South Carolina flagship computing cluster Hyperion.

■ REFERENCES

(1) Kapnistos, M.; Lang, M.; Vlassopoulos, D.; Pyckhout-Hintzen, W.; Richter, D.; Cho, D.; Chang, T.; Rubinstein, M. Unexpected power-law stress relaxation of entangled ring polymers. *Nat. Mater.* **2008**, *7*, 997−1002.

(2) Halverson, J. D.; Lee, W. B.; Grest, G. S.; Grosberg, A. Y.; Kremer, K. Molecular dynamics simulation study of nonconcatenated ring polymers in a melt. II. Dynamics. *J. Chem. Phys.* **2011**, *134*, 204905.

(3) Pasquino, R.; et al. Viscosity of ring polymer melts. *ACS Macro Lett.* **2013**, *2*, 874−878.

(4) Gooßen, S.; Brás, A. R.; Krutyeva, M.; Sharp, M.; Falus, P.; Feoktystov, A.; Gasser, U.; Pyckhout-Hintzen, W.; Wischnewski, A.; Richter, D. Molecular scale dynamics of large ring polymers. *Phys. Rev. Lett.* **2014**, *113*, 168302.

(5) Doi, Y.; Matsubara, K.; Ohta, Y.; Nakano, T.; Kawaguchi, D.; Takahashi, Y.; Takano, A.; Matsushita, Y. Melt rheology of ring polystyrenes with ultrahigh purity. *Macromolecules* **2015**, *48*, 3140−3147.

(6) Ge, T.; Panyukov, S.; Rubinstein, M. Self-similar conformations and dynamics in entangled melts and solutions of nonconcatenated ring polymers. *Macromolecules* **2016**, *49*, 708−722.

(7) Tsalikis, D. G.; Mavrantzas, V. G.; Vlassopoulos, D. Analysis of slow modes in ring polymers: Threading of rings controls long-time relaxation. *ACS Macro Lett.* **2016**, *5*, 755−760.

(8) Yan, Z.-C.; Costanzo, S.; Jeong, Y.; Chang, T.; Vlassopoulos, D. Linear and nonlinear shear rheology of a marginally entangled ring polymer. *Macromolecules* **2016**, *49*, 1444−1453.

(9) Tsalikis, D. G.; Alatas, P. V.; Peristeras, L. D.; Mavrantzas, V. G. Scaling Laws for the Conformation and Viscosity of Ring Polymers in the Crossover Region around Me from Detailed Molecular Dynamics Simulations. *ACS Macro Lett.* **2018**, *7*, 916−920.

(10) Huang, Q.; Ahn, J.; Parisi, D.; Chang, T.; Hassager, O.; Panyukov, S.; Rubinstein, M.; Vlassopoulos, D. Unexpected stretching of entangled ring macromolecules. *Phys. Rev. Lett.* **2019**, *122*, 208001.

(11) O'Connor, T. C.; Ge, T.; Rubinstein, M.; Grest, G. S. Topological linking drives anomalous thickening of ring polymers in weak extensional flows. *Phys. Rev. Lett.* **2020**, *124*, 027801.

(12) Parisi, D.; Costanzo, S.; Jeong, Y.; Ahn, J.; Chang, T.; Vlassopoulos, D.; Halverson, J. D.; Kremer, K.; Ge, T.; Rubinstein, M.; Grest, G. S.; Srinin, W.; Grosberg, A. Y. Nonlinear Shear Rheology of Entangled Polymer Rings. *Macromolecules* **2021**, *54*, 2811−2827.

(13) Suzuki, J.; Takano, A.; Deguchi, T.; Matsushita, Y. Dimension of ring polymers in bulk studied by Monte-Carlo simulation and self-consistent theory. *J. Chem. Phys.* **2009**, *131*, 144902.

(14) Vettorel, T.; Grosberg, A. Y.; Kremer, K. Statistics of polymer rings in the melt: a numerical simulation study. *Phys. Biol.* **2009**, *6*, 025013.

(15) Halverson, J. D.; Lee, W. B.; Grest, G. S.; Grosberg, A. Y.; Kremer, K. Molecular dynamics simulation study of nonconcatenated ring polymers in a melt. I. Statics. *J. Chem. Phys.* **2011**, *134*, 204904.

(16) Sakaue, T. Ring polymers in melts and solutions: scaling and crossover. *Phys. Rev. Lett.* **2011**, *106*, 167802.

(17) Rosa, A.; Everaers, R. Ring polymers in the melt state: the physics of crumpling. *Phys. Rev. Lett.* **2014**, *112*, 118302.

(18) Brás, A. R.; Gooßen, S.; Krutyeva, M.; Radulescu, A.; Farago, B.; Allgaier, J.; Pyckhout-Hintzen, W.; Wischnewski, A.; Richter, D. Compact structure and non-Gaussian dynamics of ring polymer melts. *Soft Matter* **2014**, *10*, 3649−3655.

(19) Grosberg, A. Y. Annealed lattice animal model and Flory theory for the melt of non-concatenated rings: towards the physics of crumpling. *Soft Matter* **2014**, *10*, 560−565.

(20) Obukhov, S.; Johner, A.; Baschnagel, J.; Meyer, H.; Wittmer, J. P. Melt of polymer rings: The decorated loop model. *Europhys. Lett.* **2014**, *105*, 48005.

(21) Kruteva, M.; Allgaier, J.; Monkenbusch, M.; Porcar, L.; Richter, D. Self-Similar Polymer Ring Conformations Based on Elementary

Loops: A Direct Observation by SANS. *ACS Macro Lett.* **2020**, *9*, 507−511.
(22) Michieletto, D.; Marenduzzo, D.; Orlandini, E.; Alexander, G. P.; Turner, M. S. Threading dynamics of ring polymers in a gel. *ACS Macro Lett.* **2014**, *3*, 255−259.
(23) Lee, E.; Kim, S.; Jung, Y. Slowing Down of Ring Polymer Diffusion Caused by Inter-Ring Threading. *Macromol. Rapid Commun.* **2015**, *36*, 1115−1121.
(24) Smrek, J.; Grosberg, A. Y. Minimal surfaces on unconcatenated polymer rings in melt. *ACS Macro Lett.* **2016**, *5*, 750−754.
(25) Smrek, J.; Kremer, K.; Rosa, A. Threading of unconcatenated ring polymers at high concentrations: double-folded vs time-equilibrated structures. *ACS Macro Lett.* **2019**, *8*, 155−160.
(26) Michieletto, D.; Sakaue, T. Dynamical Entanglement and Cooperative Dynamics in Entangled Solutions of Ring and Linear Polymers. *ACS Macro Lett.* **2020**, *10*, 129−134.
(27) Kruteva, M.; Monkenbusch, M.; Allgaier, J.; Holderer, O.; Pasini, S.; Hoffmann, I.; Richter, D. Self-Similar Dynamics of Large Polymer Rings: A Neutron Spin Echo Study. *Phys. Rev. Lett.* **2020**, *125*, 238004.
(28) Wong, C. P. J.; Choi, P. On the diffusivity of ring polymers. *Soft Matter* **2020**, *16*, 2350−2362.
(29) Ward, I. M.; Hadley, D. W. *An Introduction to the Mechanical Properties of Solid Polymers*; John Wiley & Sons Ltd: New York, 1993.
(30) Haward, R. N.; Young, R. *The Physics of Glassy Polymers*, 2nd ed.; Springer: Netherlands, 1997.
(31) Roth, C. B. *Polymer Glasses*; CRC Press, 2016.
(32) Kramer, E. J. Microscopic and molecular fundamentals of crazing. In *Crazing in Polymers*; Kausch, H. H., Ed.; Advances in Polymer Science, Vol. *52/53*; Springer-Verlag: Berlin, Heidelberg, 1983; pp 1−56.
(33) Brown, H. R. A molecular interpretation of the toughness of glassy polymers. *Macromolecules* **1991**, *24*, 2752−2756.
(34) Kramer, E. J.; Berger, L. L. Fundamental processes of craze growth and fracture. In *Crazing in Polymers Vol. 2*; Kausch, H.-H., Ed.; Advances in Polymer Science, Vol. *91/92*; Springer: Berlin, Heidelberg, 1990; pp 1−68.
(35) Krupenkin, T. N.; Fredrickson, G. H. Crazing in two and three dimensions. 1. Two-dimensional crazing. *Macromolecules* **1999**, *32*, 5029−5035.
(36) Krupenkin, T. N.; Fredrickson, G. H. Crazing in two and three dimensions. 2. Three-dimensional crazing. *Macromolecules* **1999**, *32*, 5036−5045.
(37) Estevez, R.; Tijssens, M. G. A.; Van der Giessen, E. Modeling of the competition between shear yielding and crazing in glassy polymers. *J. Mech. Phys. Solid.* **2000**, *48*, 2585−2617.
(38) Creton, C.; Kramer, E. J.; Brown, H. R.; Hui, C.-Y. *Molecular Simulation Fracture Gel Theory*; Springer, 2001; pp 53−136.
(39) Socrate, S.; Boyce, M. C.; Lazzeri, A. A micromechanical model for multiple crazing in high impact polystyrene. *Mech. Mater.* **2001**, *33*, 155−175.
(40) Tiejun, W.; Kishimoto, K.; Notomi, M. Effect of triaxial stress constraint on the deformation and fracture of polymers. *Acta Mech. Sin.* **2002**, *18*, 480−493.
(41) Rottler, J.; Barsky, S.; Robbins, M. O. Cracks and crazes: on calculating the macroscopic fracture energy of glassy polymers from molecular simulations. *Phys. Rev. Lett.* **2002**, *89*, 148304.
(42) Rottler, J.; Robbins, M. O. Growth, microstructure, and failure of crazes in glassy polymers. *Phys. Rev. E: Stat., Nonlinear, Soft Matter Phys.* **2003**, *68*, 011801.
(43) Gearing, B. P.; Anand, L. On modeling the deformation and fracture response of glassy polymers due to shear-yielding and crazing. *Int. J. Solid Struct.* **2004**, *41*, 3125−3150.
(44) Rottler, J. Fracture in glassy polymers: a molecular modeling perspective. *J. Phys. Condens. Matter* **2009**, *21*, 463101.
(45) Deblieck, R. A. C.; Van Beek, D. J. M.; Remerie, K.; Ward, I. M. Failure mechanisms in polyolefines: The role of crazing, shear yielding and the entanglement network. *Polymer* **2011**, *52*, 2979−2990.
(46) De Focatiis, D. S. A.; Buckley, C. P. Craze initiation in glassy polymers: Quantifying the influence of molecular orientation. *Polymer* **2011**, *52*, 4045−4053.
(47) Toepperwein, G. N.; de Pablo, J. J. Cavitation and crazing in rod-containing nanocomposites. *Macromolecules* **2011**, *44*, 5498−5509.
(48) Mahajan, D. K.; Hartmaier, A. Mechanisms of crazing in glassy polymers revealed by molecular dynamics simulations. *Phys. Rev. E: Stat., Nonlinear, Soft Matter Phys.* **2012**, *86*, 021802.
(49) Cheng, S.; Johnson, L.; Wang, S.-Q. Crazing and strain localization of polycarbonate glass in creep. *Polymer* **2013**, *54*, 3363−3369.
(50) Wang, S.-Q.; Cheng, S.; Lin, P.; Li, X. A phenomenological molecular model for yielding and brittle-ductile transition of polymer glasses. *J. Chem. Phys.* **2014**, *141*, 094905.
(51) Venkatesan, S.; Basu, S. Investigations into crazing in glassy amorphous polymers through molecular dynamics simulations. *J. Mech. Phys. Solid.* **2015**, *77*, 123−145.
(52) Ge, T.; Tzoumanekas, C.; Anogiannakis, S. D.; Hoy, R. S.; Robbins, M. O. Entanglements in glassy polymer crazing: Cross-links or tubes? *Macromolecules* **2017**, *50*, 459−471.
(53) Jiang, H.; Zhang, J.; Yang, Z.; Jiang, C.; Kang, G. Modeling of competition between shear yielding and crazing in amorphous polymers' scratch. *Int. J. Solid Struct.* **2017**, *124*, 215−228.
(54) Razavi, M.; Cheng, S.; Huang, D.; Zhang, S.; Wang, S.-Q. Crazing and yielding in glassy polymers of high molecular weight. *Polymer* **2020**, *197*, 122445.
(55) Hur, K.; Winkler, R. G.; Yoon, D. Y. Comparison of ring and linear polyethylene from molecular dynamics simulations. *Macromolecules* **2006**, *39*, 3975−3977.
(56) Tsolou, G.; Stratikis, N.; Baig, C.; Stephanou, P. S.; Mavrantzas, V. G. Melt structure and dynamics of unentangled polyethylene rings: Rouse theory, atomistic molecular dynamics simulation, and comparison with the linear analogues. *Macromolecules* **2010**, *43*, 10692−10713.
(57) Hur, K.; Jeong, C.; Winkler, R. G.; Lacevic, N.; Gee, R. H.; Yoon, D. Y. Chain dynamics of ring and linear polyethylene melts from molecular dynamics simulations. *Macromolecules* **2011**, *44*, 2311−2315.
(58) Reigh, S. Y.; Yoon, D. Y. Concentration dependence of ring polymer conformations from Monte Carlo simulations. *ACS Macro Lett.* **2013**, *2*, 296−300.
(59) Tsalikis, D. G.; Koukoulas, T.; Mavrantzas, V. G.; Pasquino, R.; Vlassopoulos, D.; Pyckhout-Hintzen, W.; Wischnewski, A.; Monkenbusch, M.; Richter, D. Microscopic structure, conformation, and dynamics of ring and linear poly (ethylene oxide) melts from detailed atomistic molecular dynamics simulations: Dependence on chain length and direct comparison with experimental data. *Macromolecules* **2017**, *50*, 2565−2584.
(60) Zhang, T.; Winey, K. I.; Riggleman, R. A. Conformation and dynamics of ring polymers under symmetric thin film confinement. *J. Chem. Phys.* **2020**, *153*, 184905.
(61) Kremer, K.; Grest, G. S. Dynamics of entangled linear polymer melts: A molecular-dynamics simulation. *J. Chem. Phys.* **1990**, *92*, 5057−5086.
(62) Hsu, H.-P.; Kremer, K. Static and dynamic properties of large polymer melts in equilibrium. *J. Chem. Phys.* **2016**, *144*, 154907.
(63) Everaers, R.; Sukumaran, S. K.; Grest, G. S.; Svaneborg, C.; Sivasubramanian, A.; Kremer, K. Rheology and microscopic topology of entangled polymeric liquids. *Science* **2004**, *303*, 823−826.
(64) Auhl, R.; Everaers, R.; Grest, G. S.; Kremer, K.; Plimpton, S. J. Equilibration of long chain polymer melts in computer simulations. *J. Chem. Phys.* **2003**, *119*, 12718−12728.
(65) Stevens, M. J. Interfacial fracture between highly cross-linked polymer networks and a solid surface: effect of interfacial bond density. *Macromolecules* **2001**, *34*, 2710−2718.
(66) Ge, T.; Pierce, F.; Perahia, D.; Grest, G. S.; Robbins, M. O. Molecular dynamics simulations of polymer welding: Strength from interfacial entanglements. *Phys. Rev. Lett.* **2013**, *110*, 098301.

https://doi.org/10.1021/acs.macromol.1c01080
Macromolecules 2021, 54, 7500−7511

(67) Ge, T.; Grest, G. S.; Robbins, M. O. Structure and strength at immiscible polymer interfaces. *ACS Macro Lett.* **2013**, *2*, 882−886.
(68) Ge, T.; Grest, G. S.; Robbins, M. O. Tensile fracture of welded polymer interfaces: Miscibility, entanglements, and crazing. *Macromolecules* **2014**, *47*, 6982−6989.
(69) Ge, T.; Robbins, M. O.; Perahia, D.; Grest, G. S. Healing of polymer interfaces: Interfacial dynamics, entanglements, and strength. *Phys. Rev. E: Stat., Nonlinear, Soft Matter Phys.* **2014**, *90*, 012602.
(70) Meng, D.; Kumar, S. K.; Ge, T.; Robbins, M. O.; Grest, G. S. Crazing of nanocomposites with polymer-tethered nanoparticles. *J. Chem. Phys.* **2016**, *145*, 094902.
(71) Ethier, J. G.; Drummy, L. F.; Vaia, R. A.; Hall, L. M. Uniaxial Deformation and Crazing in Glassy Polymer-Grafted Nanoparticle Ultrathin Films. *ACS Nano* **2019**, *13*, 12816−12829.
(72) Odell, J. A.; Keller, A. Flow-induced chain fracture of isolated linear macromolecules in solution. *J. Polym. Sci., Part B: Polym. Phys.* **1986**, *24*, 1889−1916.
(73) Creton, C.; Kramer, E. J.; Hui, C. Y.; Brown, H. R. Failure mechanisms of polymer interfaces reinforced with block copolymers. *Macromolecules* **1992**, *25*, 3075−3088.
(74) Baljon, A. R. C.; Robbins, M. O. Simulations of crazing in polymer glasses: Effect of chain length and surface tension. *Macromolecules* **2001**, *34*, 4200−4209.
(75) Rottler, J.; Robbins, M. O. Jamming under tension in polymer crazes. *Phys. Rev. Lett.* **2002**, *89*, 195501.
(76) Rottler, J.; Robbins, M. O. Yield conditions for deformation of amorphous polymer glasses. *Phys. Rev. E: Stat., Nonlinear, Soft Matter Phys.* **2001**, *64*, 051801.
(77) Plimpton, S. Fast parallel algorithms for short-range molecular dynamics. *J. Comput. Phys.* **1995**, *117*, 1−19.
(78) Adolf, D.; Tirrell, M.; Prager, S. Molecular weight dependence of healing and brittle fracture in amorphous polymers above the entanglement molecular weight. *J. Polym. Sci., Polym. Phys. Ed.* **1985**, *23*, 413−427.
(79) Mikos, A. G.; Peppas, N. A. Polymer chain entanglements and brittle fracture. *J. Chem. Phys.* **1988**, *88*, 1337−1342.
(80) Wool, R. P. *Polymer Interfaces: Structure and Strength*; Hanser Publishers, 1995.
(81) Schnell, R.; Stamm, M.; Creton, C. Direct correlation between interfacial width and adhesion in glassy polymers. *Macromolecules* **1998**, *31*, 2284−2292.
(82) Tzoumanekas, C.; Theodorou, D. N. Topological analysis of linear polymer melts: a statistical approach. *Macromolecules* **2006**, *39*, 4592−4604.
(83) Anogiannakis, S. D.; Tzoumanekas, C.; Theodorou, D. N. Microscopic description of entanglements in polyethylene networks and melts: strong, weak, pairwise, and collective attributes. *Macromolecules* **2012**, *45*, 9475−9492.
(84) Pastewka, L.; Robbins, M. O. Contact between rough surfaces and a criterion for macroscopic adhesion. *Proc. Natl. Acad. Sci. U.S.A.* **2014**, *111*, 3298−3303.
(85) Yang, A. C. M.; Kramer, E. J.; Kuo, C. C.; Phoenix, S. L. Crazes in diluted entanglement networks of polystyrene. *Macromolecules* **1986**, *19*, 2020−2027.
(86) Michieletto, D.; Turner, M. S. A topologically driven glass in ring polymers. *Proc. Natl. Acad. Sci. U.S.A.* **2016**, *113*, 5195−5200.
(87) Michieletto, D.; Nahali, N.; Rosa, A. Glassiness and heterogeneous dynamics in dense solutions of ring polymers. *Phys. Rev. Lett.* **2017**, *119*, 197801.
(88) Smrek, J.; Chubak, I.; Likos, C. N.; Kremer, K. Active topological glass. *Nat. Commun.* **2020**, *11*, 26.
(89) Locatelli, E.; Bianco, V.; Malgaretti, P. Activity-Induced Collapse and Arrest of Active Polymer Rings. *Phys. Rev. Lett.* **2021**, *126*, 097801.
(90) Sánchez-Valencia, A.; Smerdova, O.; Hutchings, L. R.; De Focatiis, D. S. The roles of blending and of molecular weight distribution on craze initiation. *Macromolecules* **2017**, *50*, 9507−9514.
(91) Si, L.; Massa, M. V.; Dalnoki-Veress, K.; Brown, H. R.; Jones, R. A. L. Chain entanglement in thin freestanding polymer films. *Phys. Rev. Lett.* **2005**, *94*, 127801.

https://doi.org/10.1021/acs.macromol.1c01080
Macromolecules 2021, 54, 7500−7511